ROZPRAWY INŻYNIERSKIE • ENGINEERING TRANSACTIONS • 24 1, 171—183, 1976
Polska Akademia Nauk • Instytut Podstawowych Problemów Techniki

SLIP-LINE SOLUTIONS OF SOME AXI-SYMMETRIC PROBLEMS OF PLASTIC COMPRESSION OF CYLINDERS AND RINGS

M. GRZYMKOWSKI and Z. MRÓZ (WARSZAWA)

Two axi-symmetric problems are treated for a perfectly plastic model: indentation of cylindrical punches into a circular plate and compression of rings between rigid plates. Static and kinematic fields are determined by integrating numerically characteristic equations for stress and velocity. Bounds on limit indentation and compression pressures are computed and compared with experimentally determined pressures.

1. Basic assumptions and equations

The present paper is devoted to the analysis of plastic flow occuring during indentation of two rigid punches into a cylinder and compression of rings between two rigid platens. These two cases occur frequently in forging operations but their theoretical analysis is still insufficient. The present work complements the previous investigation on compression of short cylinders of Tresca and Coulomb materials [3, 4, 5].

Our analysis will be based on the assumption of a perfectly plastic material model satisfying Tresca yield condition and such corner stress regimes will be used for which the Haar-Kármán hypothesis is valid. A detailed discussion of field equations can be found in [1, 2] but here we quote only fundamental relations which will be used throughout the paper.

In the case of axial symmetry, the equilibrium equations take the form

$$\frac{\partial \sigma_r}{\partial r}+\frac{\partial \tau_{rz}}{\partial z}+\frac{\sigma_r-\sigma_\theta}{r}=0\,,$$

$$\frac{\partial \tau_{rz}}{\partial r}+\frac{\partial \sigma_z}{\partial z}+\frac{\tau_{rz}}{r}=0\,, \tag{1.1}$$

where σ_r, σ_z, τ_{rz} are stresses acting in the axial plane, referred to the cylindrical polar coordinate system r, θ, z and σ_θ is the circumferential stress. Here, we consider such corner regimes of the Tresca yield condition for which σ_θ equals σ_1 or σ_2 in the axial plane, where σ_1, σ_2 $(\sigma_1>\sigma_2)$ are two principal stresses in this plane. Thus the yield condition takes the form

$$\sigma_1-\sigma_2=2k\,, \quad \sigma_\theta=\sigma_1 \quad \text{or} \quad \sigma_2\,. \tag{1.2}$$

The set of equilibrium equations (1.1) together with the yield condition is hyperbolic and the stress characteristics (α, β-lines) follow the lines of maximum shearing stress in the axial plane. The characteristic relations are

$$\begin{aligned} &\alpha\text{-line:} \quad \frac{dz_\alpha}{dr_\alpha} = \operatorname{tg}\vartheta, \qquad dp - 2k d\vartheta = \frac{k}{r}(dz_\alpha \pm dr_\alpha), \\ &\beta\text{-line:} \quad \frac{dz_\beta}{dr_\beta} = -\operatorname{ctg}\vartheta, \qquad dp + 2k d\vartheta = -\frac{k}{r}(dz_\beta \mp dr_\beta), \end{aligned} \tag{1.3}$$

where $p=-(\sigma_1+\sigma_2)/2$ and dr_α, dz_α, dr_β, dz_β are projections of the length elements ds_α, ds_β of α- and β-lines on the z- and r-axes.

The velocity characteristics coincide with the α and β-lines and the characteristic relations are

$$\begin{aligned} &\alpha\text{-line:} \quad \frac{dz_\alpha}{dr_\alpha} = \operatorname{tg}\vartheta, \qquad dv_r\cos\vartheta + dv_z\sin\vartheta = -\frac{v_r}{2r}(dr_\alpha\cos\vartheta + dz_\alpha\sin\vartheta), \\ &\beta\text{-line:} \quad \frac{dz_\beta}{dr_\beta} = -\operatorname{ctg}\vartheta, \qquad dv_r\sin\vartheta - dv_z\cos\vartheta = \frac{v_r}{2r}(dz_\beta\cos\vartheta - dr_\beta\sin\vartheta), \end{aligned} \tag{1.4}$$

where v_r and v_z are velocity components along the r and z-axes.

If a line of discontinuity in the velocity field occurs in the axial plane, it corresponds to a jump in the velocity component tangential to this line and must therefore coincide with one ot the slip lines. Consider, for instance, the case when the discontinuity in v_α propagates along the α-line and the jump $\Delta v_\alpha = v_\alpha^+ - v_\alpha^-$ equals the difference of velocities across this line. The first equation (1.4) now furnishes the relation

$$\Delta v_\alpha = \frac{v_\alpha^A\sqrt{r_A}}{\sqrt{r}}, \tag{1.5}$$

where v_α^A, r_A denote the value of velocity jump and the radius of some reference point A. The jump in tangential velocity changes along the line of discontinuity according to (1.5), increasing when approaching the symmetry axis. From (1.5) it follows that the line of discontinuity cannot intersect with this axis.

When σ_θ is equal to the greater principal stress σ_1, it follows from the flow rule that the principal strain rates satisfy the inequalities

$$\dot\varepsilon_2 < 0, \quad \dot\varepsilon_1 > 0, \quad \dot\varepsilon_\theta = \frac{v_r}{r} \geqslant 0, \tag{1.6}$$

and $v_r \geqslant 0$, i.e., the radial velocity is positive. On the other hand, when $\sigma_\theta = \sigma_2$, $\sigma_2 < \sigma_1$, there is

$$\dot\varepsilon_1 > 0, \quad \dot\varepsilon_2 < 0, \quad \dot\varepsilon_\theta = \frac{v_r}{r} \leqslant 0, \tag{1.7}$$

and flow occurs with negative radial velocity. It will turn out that the inequalities (1.6) and (1.7) will not be satisfied in some regions of plastic domain. The constructed

velocity field is then kinematically admissible, although it violates the corner flow rule. It nevertheless can be used in determining the upper bound on the limit load p_l by using the relation

$$\int p_l v_0 \, dS_0 = \int \sigma_{ij} \dot{\varepsilon}_{ij} \, dV + \int \tau_s \Delta v_s \, dl_s, \tag{1.8}$$

where the right-hand terms represent the rate of dissipation within the plastic volume and on the discontinuity lines l_s, whereas the left-hand expression represents the rate of external work of a rigid tool moving with the prescribed velocity v_0 on the surface portion S_0.

2. Indentation of two punches into a circular plate

Figure 1 illustrates the problem: two rigid cylindrical punches of radii r_s are indented into a circular plate of radius $r_m > r_s$ and thickness $2h$. It turns out that the static solution for some ratios r_m/h can be constructed by decomposing it into two separate problems: i) expansion of an annular disk $r_s \leqslant r \leqslant r_m$ by the radial pressure $\sigma_r = -q$ acting on the boundary defined by OA, ii) compression of a cylinder $0 \leqslant r \leqslant r_s$ by two punches and the lateral pressure $\sigma_r = -q$ on OA. The static field for the disk problem can be determined analytically, whereas the slip-line solution will be determined for the cylinder problem.

Let us first discuss the solution within the external ring. For the Tresca yield condition, we have $\sigma_z = 0$, $\sigma_\theta - \sigma_r = 2k$ and the equilibrium equation (1.1) furnishes

$$\begin{aligned} &\sigma_r = -2k \ln \frac{r_p}{r}, && r_s \leqslant r \leqslant r_p, \\ &\sigma_\theta = 2k \left(1 - \ln \frac{r_p}{r}\right), && \sigma_r = \sigma_\theta = 0, \\ &&& r_p \leqslant r \leqslant r_m. \end{aligned} \tag{2.1}$$

Hence

$$q = -\sigma_r|_{r=r_s} = 2k \ln \frac{r_p}{r_s}. \tag{2.2}$$

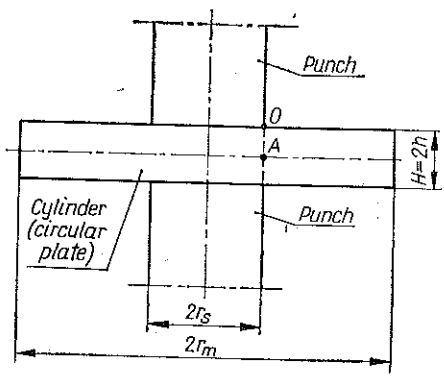

Fig. 1. Indentation of two rigid cylindrical punches into a circular plate

In writing (2.1) we assume that $\sigma_r = 0$ for $r = r_p$, where r_p denotes the radius of the plastic region. The value of r_p follows from the kinematic solution and the velocity field of Fig. 2 implies $r_p = r_s + 2h$ when $r_m > r_s + 2h$ and $r_p = r_m$ when $r_m < r_s + 2h$. Since the stress q should vary within the limits $0 \leqslant q \leqslant 2k$, Eq. (2.2) provides the inequality

$$\frac{r_p}{r_s} = \frac{2h}{r_s} < e = 2.718. \tag{2.3}$$

Now, let us pass to the solution of the stress equations for a cylinder $0 \leqslant r \leqslant r_s$. Figures 2a, b show the net of stress characteristics for $r_s/h=1.5$, 3 and $r_m > r_s+2h$ so that $r_p=r_s+2h$. Fig. 2c presents the case $r_s/h=1.5$, $r_m < r_s+2h$. In view of the symmetry of the problem, the solution is presented in the first quadrant of the r,

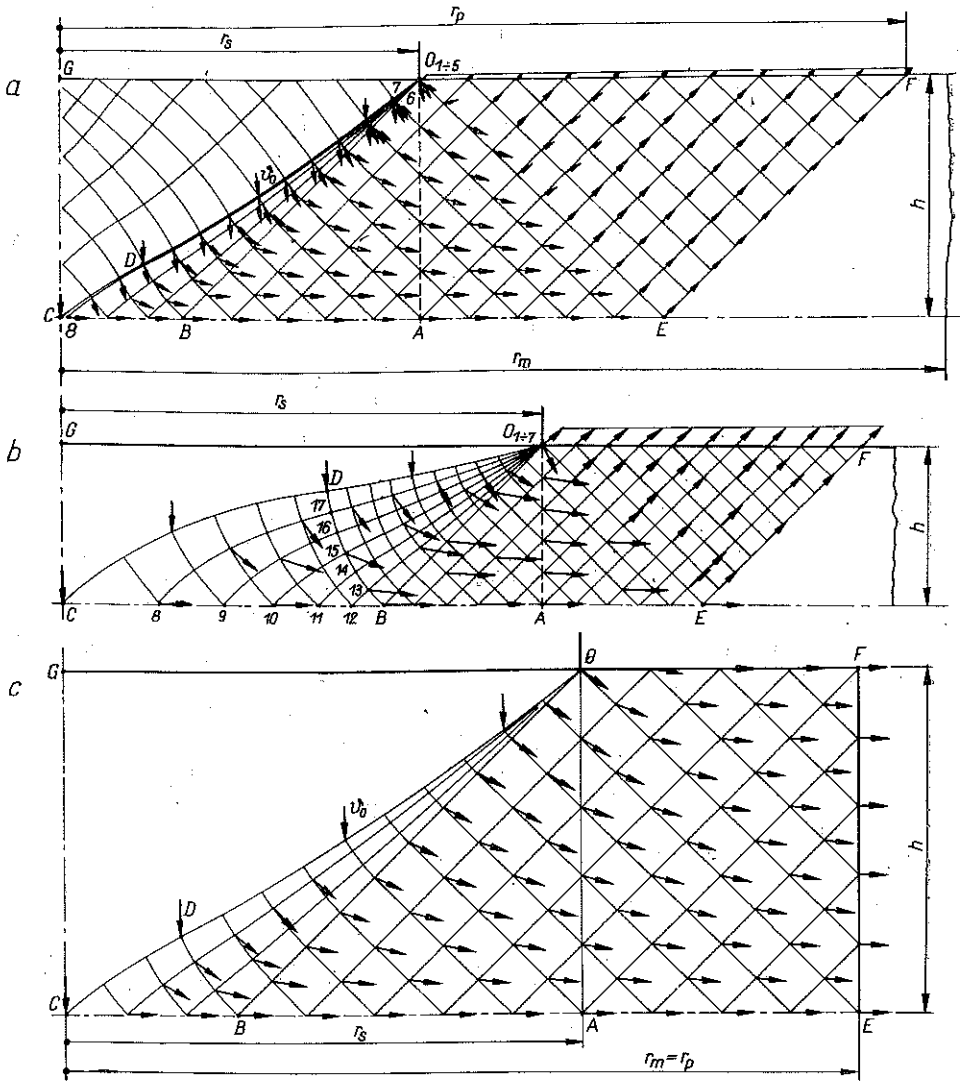

Fig. 2. Characteristic meshes and velocity fields for characteristic ratios:
a) $r_s/h=1.5$, $r_m \geqslant r_s+2h$; b) $r_s/h=3$, $r_m \geqslant r_s+2h$; c) $r_s/h=1.5$, $r_m \leqslant r_s+2h$

z-plane. Within the region OAB the stress state is uniform, $\sigma_\theta=\sigma_r=-q$, $\sigma_z=-(2k+q)$, $p=q+k$, $\vartheta=3/4\pi$. The stress state in the centred fan OBD and the region BDC is found by integrating stress equations (1.3) and satisfying proper boundary conditions. Thus for OBD, the stress state on OB and the condition at

the singular point O ($p-2k\vartheta=\text{const}$) provide the solution within the whole domain. Similarly, the conditions on BD and BC ($\vartheta=3/4\pi$) provide the solution within DBC. The stress field can be extended beyond ODC into the rigid region $ODCG$, Fig. 2a, but the vertical resultant force of indentation can be computed by integrating vertical traction along ODC

$$P=\int 2\pi r_d(\sigma_z\, dr_d+\tau_{rz}\, dz_d), \tag{2.4}$$

where dr_d, dz_d denote the length elements of the characteristic line ODC. The Eq. (2.4) provides the lower bound to the limit indentation force.

The velocity field is constructed by assuming that the portion $ODCG$ moves like a rigid body with the plate and the discontinuity lines OE and EF occur within the external region. Thus on ODC there is $v_z=-v_0$, $v_r=0$ and on CBA we have $v_z=0$, $v_r>0$. Using the characteristic relations (1.4), the velocity field is determined within $ODCBAEF$. Near the point C, the analytic expression for velocities can be used [1]:

$$v_r=\frac{2v_0}{\pi}(1-\operatorname{tg}^2\psi)^{1/2},\qquad v_z=-\frac{2v_0}{\pi}\arccos(\operatorname{tg}\psi), \tag{2.5}$$

where ψ is the inclination of the radius vector from C to the r-axis. At E the velocity v_E is decomposed along two discontinuity lines OE and EF: $\Delta v_E^{OE}=v_E\frac{\sqrt{2}}{2}$, $\Delta v_E^{EF}=v_E\frac{\sqrt{2}}{2}$ and the variation of velocity jumps along OE and EF is determined from (1.5). Figure 3 shows the deformed rectangular net during indentation for $r_s/h=1.5$, $r_m>r_s+2h$ and the velocity hodograph for $r_s/h=3$ is shown in Fig. 4. It turns

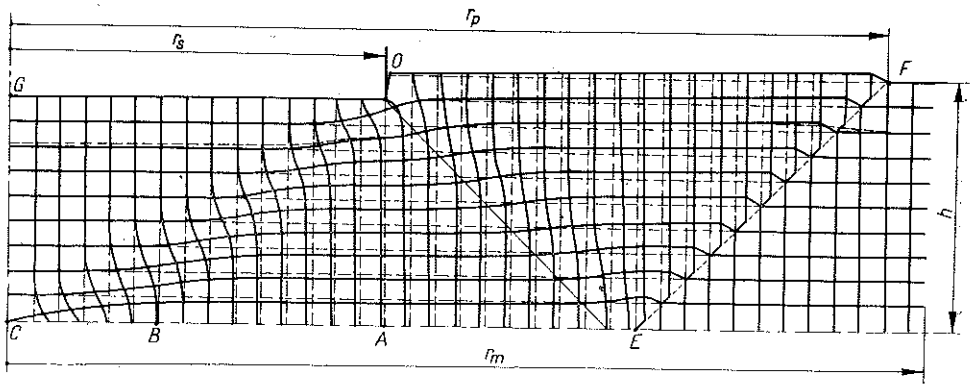

Fig. 3. Theoretically predicted deformation of an initially square mesh for a cylinder $r_s/h=1.5$ $r_m>r_s+2h$

out that inequalities (1.6) are violated within AOB and the velocity field provides only an upper bound on the indentation force-since it does not correspond to the exact solution for the Tresca material. Using (1.8), the upper bound can be determined numerically once the velocity field has been constructed. Figure 5 presents

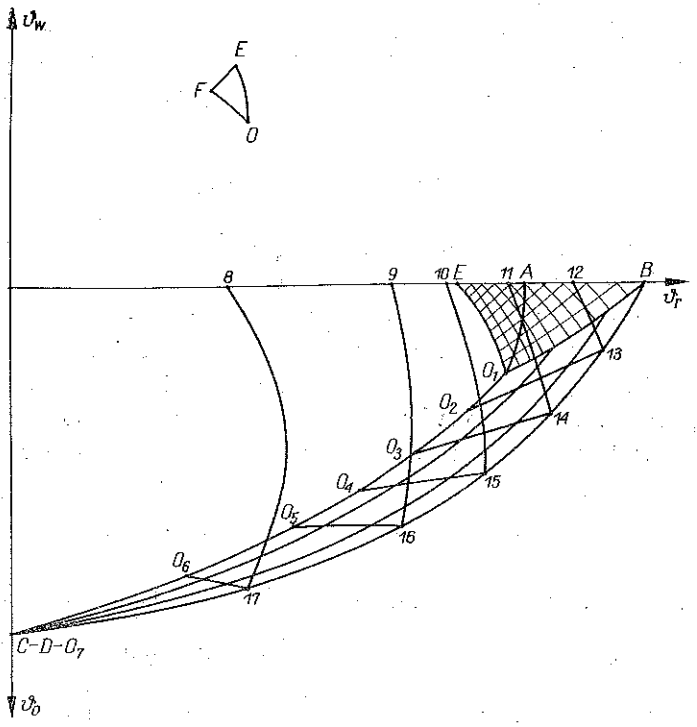

Fig. 4. Hodograph for the cylinder of height $h=5$ mm, $r_s/h=3$

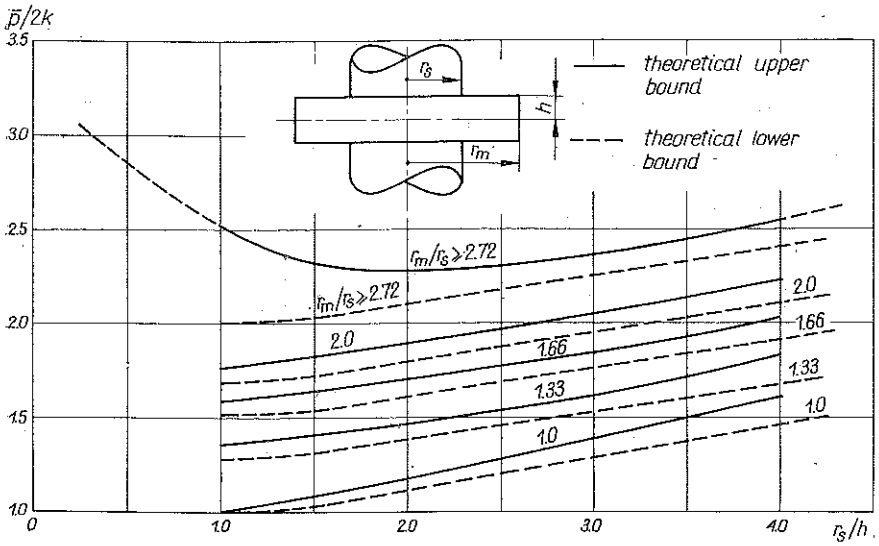

Fig. 5. Upper and lower bounds to indentation pressures predicted by the method of characteristics

both upper and lower bounds to the limit punch pressure. It is seen that bounds are fairly close thus indicating that the velocity and stress fields are good approximations to the complete solution.

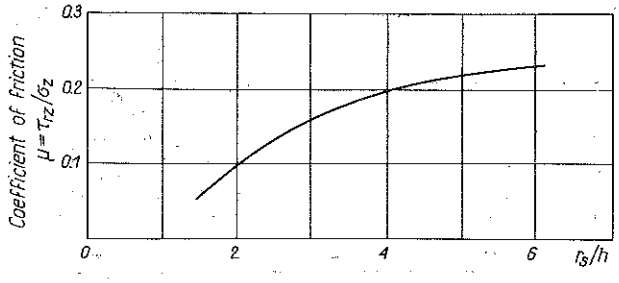

Fig. 6. The required coefficient of friction at the contact interface between punch and cylinder

The static solution is valid provided sufficient friction coefficient exists between the cylinder and the punch. Evaluating this coefficient at 0, we obtain the diagram shown in Fig. 6. Thus for smaller friction coefficients, the limit characteristic ODC would form a greater angle with OG and the plastic region would be extended above ODC. This type of solution was discussed in [3].

3. Compression of rings between rigid plates

Figure 7 presents the ring dimensions and the loading plate. This type of test is often used to determine the coefficient of friction by measuring the radius separating the inner zone moving toward the symmetry axis from the external zone moving outwards. Simplified analyses of this problem can be found in [6, 7], where equilibrium conditions were satisfied only globally for thin slices in which the stress state was assumed as uniform along vertical direction. Here, the stress field will be determined using the stress characteristics, but the solution will not be complete, since it is not shown that the stress field can be continued into the rigid region. Moreover, we will not discuss different friction conditions at the interface, restricting our analysis to sufficiently high friction coefficients for which the presented solution is valid.

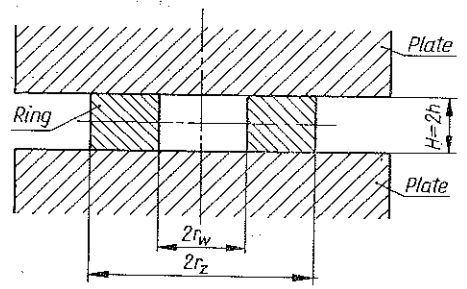

Fig. 7. Compression of rings between two rigid plates

Figure 8 presents the slip line fields with velocity vectors. Now, in the region BKG there is $\sigma_\theta = \sigma_2$ and $v_r < 0$, whereas within the region $DCFGE$ there is $\sigma_\theta = \sigma_1$ and $v_r > 0$. At G there should be continuity of σ_r although σ_θ may vary discontinuously.

This continuity condition provides the position of point G and completes the static solution. We start from the boundaries BK and CD by determining the solution within BKJ and CDE and next in the centred fans EFC and BHJ. The angles of centred fans are governed by the continuity conditions at G. The velocity field is constructed by assuming that BGC moves vertically with the plate and both GFC

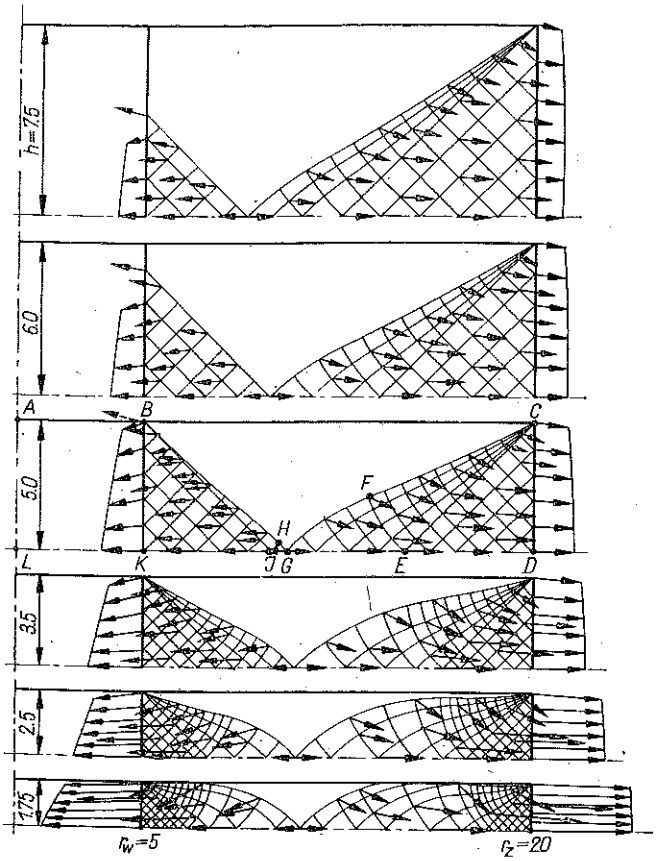

Fig. 8. Characteristic meshes and velocity fields for rings of constant radii r_z, r_w but varying thickness h

and BHG are discontinuity lines. It turns out that the inequalities (1.6) and (1.7) are violated within BKJ and DCE. Hence the constructed velocity field is kinematically admissible and can be used to provide an upper bound to the plate pressure. Figure 9 presents bounds to this pressure derived from the velocity and stress fields. Whereas the velocity field provides an upper bound, the stress field provides an estimate which should not necessarily represent a lower bound, since continuation of the stress field into the rigid region may not exist. It is seen that bounds are fairly close, diverging for increasing ratios r_z/h and r_z/r_w. The value of a neutral radius r_n defining separation of zones of plastic flow toward the symmetry axis and in the outward direction can also be determined from the static solution.

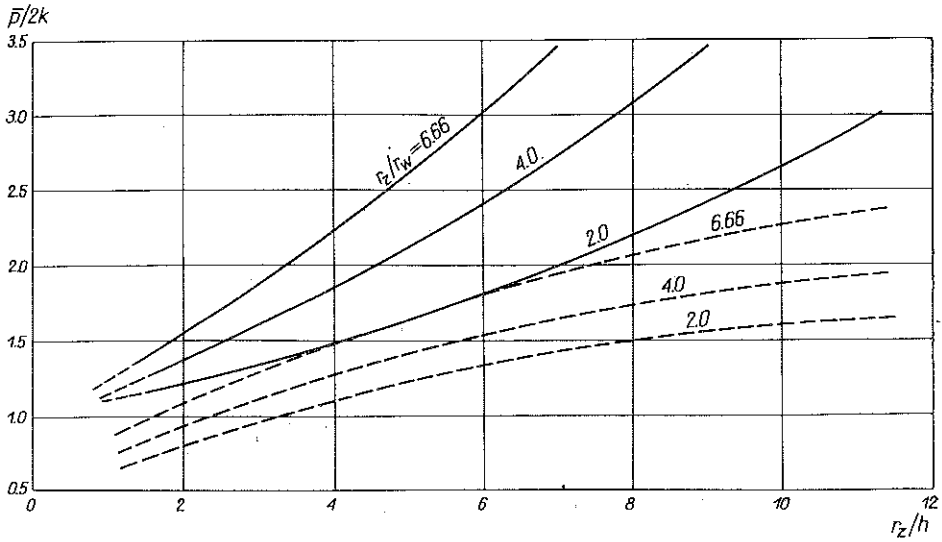

Fig. 9. Upper and lower bound to plate pressure predicted from slip-line fields:
——— upper bound, — — — lower bound

Similarly as previously, the static solutions are valid provided a proper coefficient of friction exists between the plate and the ring. Figure 10 shows the required values of μ evaluated at B and C. Thus is order to satisfy the validity of these solutions, a sufficiently large friction coefficient at the interface BC should be assured.

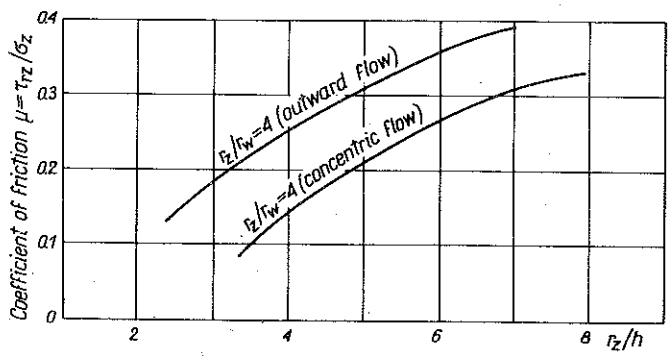

Fig. 10. The required coefficient of friction at the contact interface (of ring and plates) evaluated at B and C

4. Experimental results

Compression tests were carried out using lead disks and rings. The conventional yield limit was assumed as that value of stress which corresponds to $\varepsilon=0.1$ per cent of the offset strain. This value of stress corresponds also to the point of maximum curvature of the stress-strain curve.

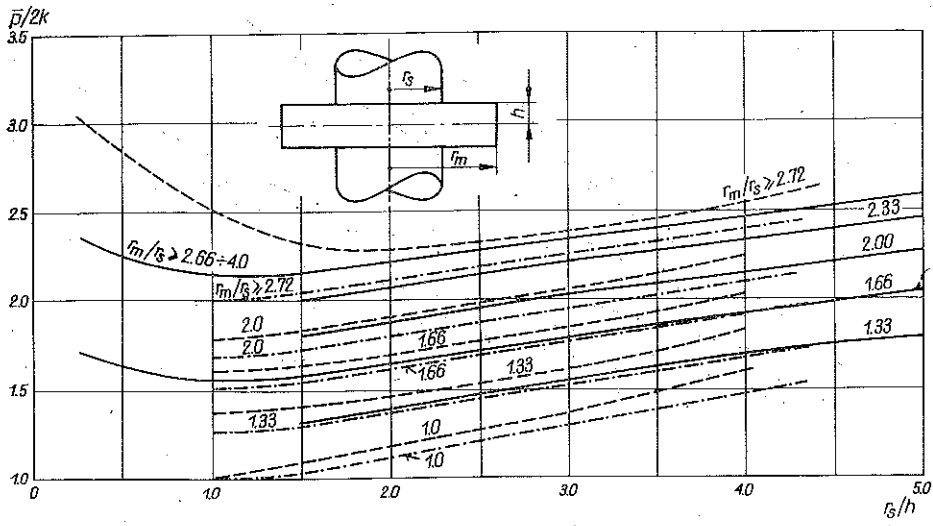

Fig. 11. Theoretical bounds and experimental results for indentation test of rigid punches into the cylinder:

——— experimental curve, — — — upper bound, —·—·—·— lower bound

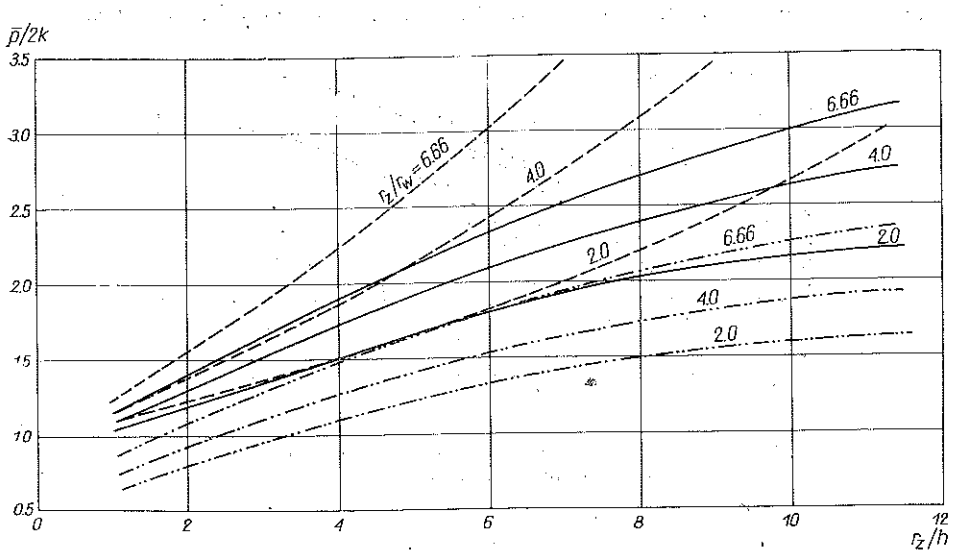

Fig. 12. Theoretical bounds and experimentally determined pressures for the case of compression of rings:

——— experimental curve, — — — upper bound, — ·· — ·· lower bound

Tests were carried out using a special experimental rig connected with a hydraulic testing machine allowing for the exact measurement of load and displacement of compressing plates. The conventional limit pressure was determined for different values of mean plastic strain $\varepsilon_m = \Delta h/h$. Figures 11 and 12 show experimental data plotted for compression of cylinders and rings corresponding to the mean plastic strain $\varepsilon_m = 0.1$ per cent. It is seen that a fairly good correlation exists between experimentally determined pressures and theoretical bounds, although for the case

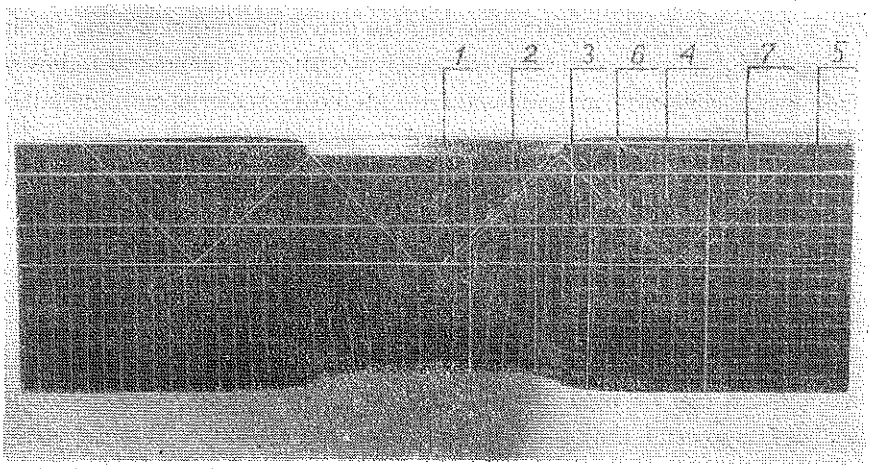

Fig. 13. Deformation of an initially square mesh on the cylinder $r_s/h = 1$, $r_m > r_s + 2h$

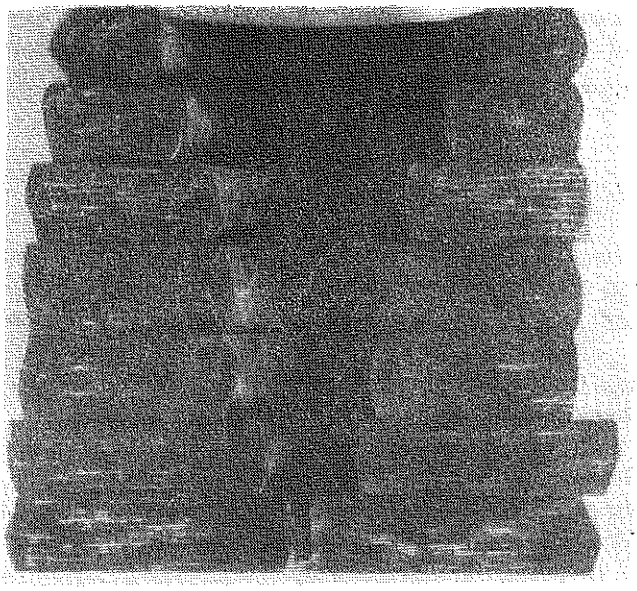

Fig. 14. Deformation of rings corresponding to mean strain $\varepsilon_m = 0.35$

of rings this agreement is poorer for larger ratios r_z/h. However, the experimental curves lie between static and kinematic bounds.

The mode of flow was observed by splitting the cylinders along the diameter plane and inserting a square grid on one portion of the cut. Figure 13 shows the deformation of an initially square grid for $r_m/r_s > 3$. Although a quantitative comparison between theoretical and experimental velocity was not carried out, the observed deformation mode agrees qualitatively with the theoretical velocity field. In particular, the theoretically predicted rigid regions *1* and *5* and zones of intensive shear *2*, *6*, *7* can be identified when studying the grid deformation. Figure 14 shows a set of split rings after the compression test. It is seen that the neutral radius separates the zones of concentric and outward flow. Moreover, material portions adhering to rigid plates behave essentially as rigid and move vertically with the plates during compression.

5. Concluding remarks

Although more accurate analysis would require incremental solution of boundary-value problems with account for elastic strains and hardening effects, the method of characteristics can be used in numerous cases in order to predict limit loads and modes of flow even if the complete solutions cannot be found. Thus the presented analysis of two problems seems to be more accurate than approximate engineering treatments using Schroeder and Webster [6] simplified approach. Whereas the latter approach neglected all details of plastic flow concentrated on discontinuity lines and provided only rough estimate of limit loads, the present approach provides also useful information on the velocity field. Comparison of these two approaches was discussed in [3, 4].

References

1. R. T. Shield, *On the plastic flow of metals under conditions of axial symmetry*, Proc. Roy. Soc., ser. A, vol. **233**, 267–287, 1955.
2. Z. Mróz, *Graphical solution of axially symmetric problems of plastic flow*, ZAMP, **18**, 219–236, 1967.
3. K. Kwaszczyńska, Z. Mróz, *A theoretical analysis of plastic compression of short circular cylinders*, Arch. Mech. Stos., **19**, 787–797, 1967.
4. Z. Mróz, K. Kwaszczyńska, *Axially symmetric plastic flow of soils treated by the graphical method*, Arch. Inż. Lądowej, **14**, 1969.
5. K. Kwaszczyńska, Z. Mróz, A. Drescher, *Analysis of compression of short cylinders of Coulomb material*, Int. J. Mech. Sci., **11**, 145–158, 1969.
6. W. Schröeder, D. A. Webster, *Press forging of thin sections: effect of friction area, and thickness on pressure required*, J. Appl. Mech., **16**, 289–294, 1949.
7. B. Avitzur, *Forging of hollow discs*, Israel J. Technology, **2**, 1964.

STRESZCZENIE

ROZWIĄZANIA METODĄ CHARAKTERYSTYK PEWNYCH OSIOWO-SYMETRYCZNYCH ZAGADNIEŃ PLASTYCZNEGO ŚCISKANIA WALCÓW I PIERŚCIENI

W pracy rozpatrzono dwa zagadnienia: wciskania sztywnych stempli cylindrycznych w kołową płytę oraz ściskanie pierścieni pomiędzy sztywnymi płytami. Rozwiązania skonstruowano dla idealnie plastycznego materiału, całkując numerycznie równania charakterystyczne dla naprężeń i prędkości. Przeprowadzone badania doświadczalne miały na celu weryfikację wyników teoretycznych zarówno jeśli chodzi o wartość granicznego nacisku jak i mechanizmu płynięcia. Uzyskano dość dobrą zgodność pomiędzy wynikami teoretycznymi i doświadczalnymi.

Резюме

РЕШЕНИЯ МЕТОДОМ ХАРАКТЕРИСТИК НЕКАТОРЫХ ОСЕСИММЕТРИЧЕСКИХ ЗАДАЧ ПЛАСТИЧЕСКОГО СЖАТИЯ ЦИЛИНДРОВ И КОЛЕЦ

В работе рассмотрены два вопроса: вдавливание жестких цилиндрических штампов в круговую плиту, а также сжатие колец между жесткими плитами. Решения построены для идеально пластического материала, интегрируя численно характеристические уравнения для напряжений и скоростей. Проведенные экспериментальные исследования имели своей целью проверку теоретических результатов, так если рассматривается предельное значение нажима, как и механизм течения. Получено довольно хорошее совпадение между теоретическими и экспериментальными результатами.

INSTITUTE OF FUNDAMENTAL TECHNOLOGICAL RESEARCH
and
TECHNICAL UNIVERSITY OF WARSAW

Received July 2, 1975.